

Explicit near-optimal quantum algorithm for solving the advection-diffusion equation

I. Novikau¹ and I. Joseph¹

Lawrence Livermore National Laboratory, Livermore, California 94550, USA

(*Electronic mail: novikau1@llnl.gov)

(Dated: 22 January 2025)

An explicit near-optimal quantum algorithm is proposed for modeling dissipative initial-value problems. This method, based on the Linear Combination of Hamiltonian Simulations (LCHS), approximates a target nonunitary operator as a weighted sum of Hamiltonian evolutions, thereby emulating a dissipative problem by mixing various time scales. We propose an efficient encoding of this algorithm into a quantum circuit based on a simple coordinate transformation that turns the dependence on the summation index into a trigonometric function and significantly simplifies block-encoding. The resulting circuit has high success probability and scales logarithmically with the number of terms in the LCHS sum and linearly with time. We verify the quantum circuit and its scaling by simulating it on a digital emulator of fault-tolerant quantum computers and, as a test problem, solve the advection-diffusion equation. The proposed algorithm can be used for modeling a wide class of nonunitary initial-value problems including the Liouville equation and linear embeddings of nonlinear systems.

I. INTRODUCTION

Precise modeling of complex dynamics characterized by multiple scales in space and time needs high spatial resolution. As a result, accurate simulations of many classical problems of practical interest require large amounts of numerical resources. This significantly limits the number of problems that can be simulated on classical computers, and it seems suitable to consider quantum computers (QCs) as possible candidates for modeling these sorts of problems. By leveraging quantum effects such as entanglement and superposition of quantum states, QCs can process exponentially many complex numbers in parallel. Moreover, in advanced quantum algorithms for solving differential equations, the number of operations grows polynomially or even exponentially more slowly than in the corresponding classical methods. Yet, quantum computers can operate only with linear unitary operators that makes quantum simulations of dissipative problems challenging.

To solve dissipative differential equations, one can transform them into a system of linear equations¹ $M\psi = b$ with a dilated matrix M . The scaling of the matrix condition number κ_M on the integration time depends on the Courant-Friedrichs-Lewy convergence condition and, for instance, is quadratic for the advection-diffusion or heat equations,² which have second-order spatial derivatives. The linear system can be solved by advanced quantum linear system algorithms such as those based on variable-time amplitude amplification^{3–5} or discrete adiabatic theorem,^{6,7} whose query complexity is linear with the condition number. More precisely, the number of calls to the oracle encoding M and to the oracle encoding the right-hand-side vector b is linear with κ_M .

Another option is to use the time-marching method,⁸ whose success probability is maintained by using a combination of the uniform singular value amplification and compression gadgets. Generally, this algorithm scales quadratically with the simulated time. In Ref. 9, it was shown how to solve the advection-diffusion equation with the time-

marching technique having linear complexity with time and high success probability. However, it is not clear whether this method would preserve the near-optimal scaling if the normalized advection-like component of the time-marching matrix cannot be block-encoded keeping the spectral norm of the encoded matrix equal to one.

One can also use hybrid classical-quantum methods for solving dissipative problems on quantum computers as proposed, for instance, in Ref. 10 and 11. Yet, the hybrid methods usually suffer from the bottleneck related to the repetitive input/output (I/O) data transfer between classical and quantum processors.

An alternative approach is based on recasting a nonunitary operator associated with dissipative dynamics into a combination of unitary evolution operators integrated over some additional Fourier space. This technique was initially proposed in Refs. 12–16 and is called “Schrödingerization” or Linear Combination of Hamiltonian Simulations (LCHS). The explicit implementation of the LCHS circuit and its numerical emulation was given in Ref. 17. Recently, the LCHS algorithm¹⁸ was advanced by exponentially improving its query complexity with respect to the truncation error ϵ_{LCHS} . In this work, we propose an explicit quantum circuit of the improved LCHS method characterized by linear query complexity with the integration time t and logarithmic complexity with the truncation error ϵ_{LCHS} . We simulate the LCHS circuit on a digital emulator of fault-tolerant quantum computers and verify the circuit by modeling the advection-diffusion equation. In these simulations, we demonstrate the near-optimal scaling of the improved LCHS algorithm and its high success probability.

This paper is organized as follows. In Sec. II A, we review the LCHS method with an improved kernel and explain in detail how this algorithm can be mapped on a quantum circuit. In Sec. III, we test the LCHS circuit by modeling the advection-diffusion equation and analyze the algorithm scaling, precision, and the circuit success probability. In Sec. IV, we summarize the main results of this paper.

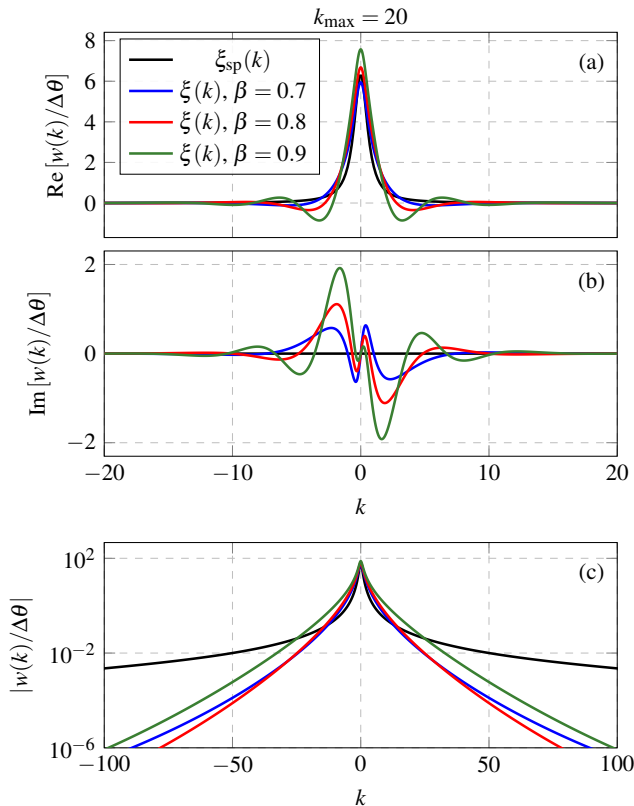


FIG. 1: Plots showing the real (a) and imaginary (b) components of the LCHS weights for the special case (6) (black line) and the improved kernel (5) with various β (colored lines). (c): Absolute values of the LCHS weights.

II. IMPROVED LINEAR COMBINATION OF HAMILTONIAN SIMULATIONS (LCHS)

A. Overview

We consider a linear differential equation with a non-Hermitian time-independent generator A

$$\partial_t \psi(t, x) = -A \psi(t, x). \quad (1)$$

Here, the evolution in time of the variable $\psi(t, x)$ is described by the nonunitary operator e^{-At} :

$$\psi(t, x) = e^{-At} \psi(0, x), \quad (2)$$

where $\psi(0, x)$ encodes initial conditions. The initial-value problem (2) can be solved by LCHS^{16,18} which represents the nonunitary operator e^{-At} as a weighted superposition of Hamiltonian evolutions integrated over additional Fourier space

$$e^{-At} = \int_{\mathbb{R}} \frac{\xi(k)}{1 - ik} e^{-i(A_H + kA_L)t} dk, \quad (3)$$

where the original generator A has been separated into Hermitian matrices

$$A = A_L + iA_H, \quad (4a)$$

$$A_L = (A + A^\dagger)/2, \quad (4b)$$

$$A_H = (A - A^\dagger)/(2i). \quad (4c)$$

Equation (3) is valid as long as A_L is positive semi-definite. The kernel $\xi(k)$ has the following form:¹⁸

$$\xi(k) = \frac{1}{2\pi e^{-2\beta} \exp([1 + ik]^\beta)}, \quad (5)$$

with the real scalar $\beta \in (0, 1)$. The LCHS algorithm with the special case of the kernel $\xi(k)$ equal to

$$\xi_{\text{sp}}(k) = \frac{1}{\pi(1 + ik)} \quad (6)$$

was numerically tested in Ref. 17. It corresponds to the original LCHS method described in Ref. 16 and is equivalent to the Schrödingerization algorithm.¹⁹

To efficiently map the LCHS equation (3) onto a quantum circuit, it is beneficial to apply the following coordinate transformation:¹⁷

$$k = k_{\text{max}} \sin(\theta). \quad (7)$$

This allows one to recast the dependence on the Fourier coordinate k as a trigonometric function, $\sin(\theta)$, which is easy to block-encode.

The LCHS computation (3) of the nonunitary operator e^{-At} is exact when one works in infinite Fourier space. Yet, to simulate Eq. (2) numerically, one must truncate Fourier space, i.e. by imposing $|k| < k_{\text{max}}$ and by discretizing the space with a grid with $N_k = 2^{n_k}$ points. In this case, the transformation (7) becomes

$$k_j = k_{\text{max}} \sin(\theta_j), \quad (8)$$

where the discretized angle θ_j is

$$\theta_j = -\frac{\pi}{2} + j\Delta\theta, \quad \Delta\theta = \frac{\pi}{N_k - 1}, \quad j = 0, 1, \dots, N_k - 1. \quad (9)$$

After the truncation of the Fourier space, one obtains a discretized version of the initial-value problem (2),

$$\psi(t, x) = U_{\text{LCHS}} \psi(0, x) + \epsilon_{\text{LCHS}}, \quad (10)$$

where ϵ_{LCHS} is the truncation error. The discretized LCHS operator U_{LCHS} approximates the nonunitary operator e^{-At} as

$$e^{-At} \approx U_{\text{LCHS}} = \sum_{j=0}^{N_k-1} w_j V_j(t), \quad (11)$$

where each unitary V_j ,

$$V_j(t) = e^{-iC_j t}, \quad (12)$$

depends on the θ -dependent Hermitian matrix C_j ,

$$C_j = A_H + \sin(\theta_j) B_m, \quad (13a)$$

$$B_m = k_{\text{max}} A_L, \quad (13b)$$

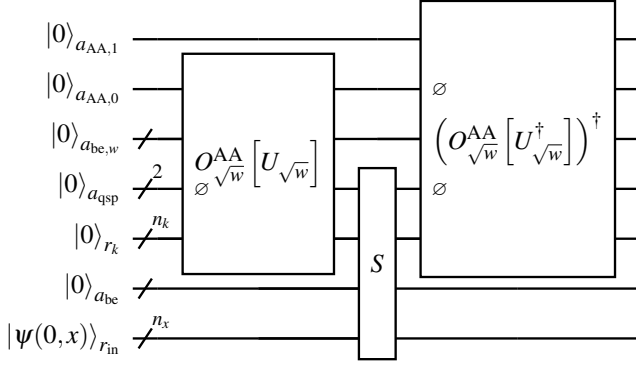


FIG. 2: LCU circuit for solving the LCHS equation (10). The selector is shown in Fig. 3. The symbol \emptyset indicates that the corresponding qubits are not used by the indicated subcircuits.

and the sum (11) is weighted by the complex coefficients w_j ,

$$w_j = \frac{k_{\max} \cos(\theta_j) \Delta\theta \xi(k_j)}{1 - ik_j}. \quad (14)$$

These weights become real, when the special kernel (6) is applied. The shape of the LCHS weights w_j computed with the improved and special kernels, Eq. (5) and Eq. (6), correspondingly, are shown in Fig. 1. One can see that the real and imaginary components of the complex weights built with the improved kernel ξ are functions of definite parity. This means that each component can be constructed by using a single QSVT circuit. Also, as can be seen from Fig. 1c, the improved kernel causes the weights to decay exponentially faster than in the special case (6). According to Ref. 18 and as is also demonstrated later in this paper, this results in the exponential decay of the truncation error ϵ_{LCHS} with k_{\max} :

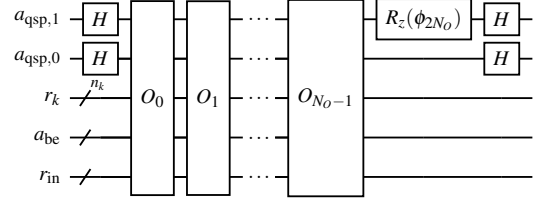
$$\epsilon_{\text{LCHS}} = \mathcal{O}\left(e^{-k_{\max}^\beta}\right). \quad (15)$$

At the same time, the truncation error in the discretized LCHS computation (10) with the special kernel ξ_{sp} is only inversely proportional to k_{\max} .^{16,17}

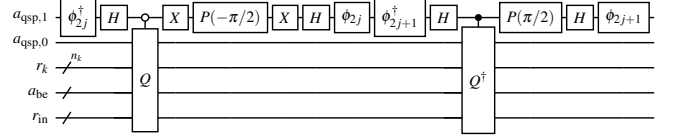
$$\epsilon_{\text{LCHS}} = \mathcal{O}(k_{\max}^{-1}). \quad (16)$$

B. LCHS circuit

The discretized LCHS transformation is expressed in the form of a weighted sum, Eq. (11). As such, it can be mapped on a Linear Combination of Unitaries (LCU) circuit as schematically shown in Fig. 2. There, the oracles $O_{\sqrt{w}}^{\text{AA}}[U_{\sqrt{w}}]$ and $(O_{\sqrt{w}}^{\text{AA}}[U_{\sqrt{w}}^\dagger])^\dagger$ compute the LCHS weights (14), and the oracle S called selector computes N_k unitaries V_j . The register r_k is used to encode the dependence on the Fourier coordinate k_j , expressed as the sine function of the angles θ_j according to Eq. (8). The ancillary qubits a_{qsp} and a_{be} are used for the construction of the selector and for block-encoding



(a) LCHS selector as a QSP circuit



(b) Operator O_j

FIG. 3: (a): Circuit of the selector S for computing N_k unitaries V_j [Eq. (12)]. The selector is represented by a single QSP^{20,21} circuit consisting of N_O operators O_j . The number N_O depends on the simulated time length t . (b): Circuit of the operator O_j for some $j = 0, 1, \dots, N_O - 1$. The operator depends on two QSP angles, ϕ_{2j} and ϕ_{2j+1} . Here, the gates schematically denoted as ϕ_l indicate the rotations $R_z(\phi_l)$. The iterate Q is shown in Fig. 4

the matrices C_j , Eq. (13). The ancillary register $a_{\text{be},w}$ is used by both oracles $O_{\sqrt{w}}^{\text{AA}}[U_{\sqrt{w}}]$ and $(O_{\sqrt{w}}^{\text{AA}}[U_{\sqrt{w}}^\dagger])^\dagger$ for computing the LCHS weights. In addition, the oracles $O_{\sqrt{w}}^{\text{AA}}[U_{\sqrt{w}}]$ and $(O_{\sqrt{w}}^{\text{AA}}[U_{\sqrt{w}}^\dagger])^\dagger$ use the ancillae $a_{\text{AA},0}$ and $a_{\text{AA},1}$, correspondingly, for amplitude amplification (AA) of the computed weights. Finally, the register r_{in} encodes the initial condition $\psi(0,x)$, which should be precomputed by some additional initialization subcircuit. The same register outputs the result, $\psi(t,x)$, entangled with the zero state of all ancillary qubits and the register r_k .

The complex LCHS weights can be computed by two QSVT circuits combined by an LCU. There, each QSVT can be implemented in the manner explained in detail in Ref. 17. In particular, the oracle $O_{\sqrt{w}}^{\text{AA}}[U_{\sqrt{w}}]$ includes as a subcircuit the oracle $U_{\sqrt{w}}$, which computes the complex values $\sqrt{w_j}$ by using the combined QSVT-LCU circuit. An alternative approach for the computation of $\sqrt{w_j}$ is a tensor-network-based technique described in Ref. 22. In our numerical emulations, we use a direct exact brute-force computation of the LCHS weights to minimize the number of ancillary qubits in the circuit. In this case, the oracle $U_{\sqrt{w}}$ is constructed as a sequence of N_k combined rotations $R_y(\phi_{y,j})R_z(\phi_{z,j})$ where $\phi_{y,j} = 2 \arccos(|\sqrt{w_j}|)$ and $\phi_{z,j} = -2 \arg(\sqrt{w_j})$. After the weight computation, one should apply AA to amplify the success probability of the oracle $U_{\sqrt{w}}$, thereby boosting the success probability of the entire LCHS circuit 2. The amplification is implemented by the oracle $O_{\sqrt{w}}^{\text{AA}}[U_{\sqrt{w}}]$ and can be accomplished by using the standard AA technique.²³ This was explained in detail in Ref. 17. In particular, AA requires $2N_{\text{AA}}$ repetitions of the subcircuit $U_{\sqrt{w}}$. For instance, for

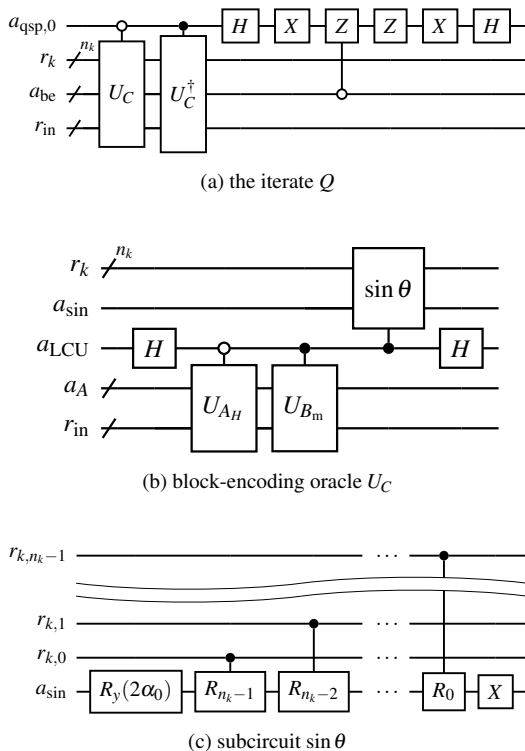


FIG. 4: (a): Circuit of the iterate Q used in the selector 3. Note that the qubitization is performed only with respect to the ancillary register a_{be} independently of the register r_k , although the latter is also used by the block-encoding oracle U_C . (b): Circuit of the block-encoding oracle U_C encoding C_j , Eq (13). The implementation of the subcircuits U_{A_H} and U_{B_m} depends on the structure of A . The registers a_A , a_{LCU} , and a_{sin} are different parts of the register a_{be} used in Fig. 4a.

(c): Circuit encoding the function $\sin(\theta_j)$ for $j = 0, 1, \dots, N_k - 1$. Here, $R_l = R_y(2\alpha_l/2^l)$, $\alpha_0 = -\pi/2$, and $\alpha_1 = |\alpha_0|N_k/(N_k - 1)$.

$k_{\max} = 40$, one has $N_{AA} = 30$ and $N_{AA} = 43$ for $n_k = 11$ and $n_k = 12$, correspondingly. An important remark here is that AA does not concern the selector S which is the most computationally intensive component of the LCHS circuit. Therefore, one performs only $\mathcal{O}(N_{AA})$ repetitions of $U_{\sqrt{w}}$ without touching the selector. Apart from this, since S makes the dominant contribution to the complexity of the LCHS circuit and scales with time, the choice in the implementation of $U_{\sqrt{w}}$ has a small effect on the length of the entire LCHS circuit.

The selector S is implemented as a single QSP^{20,21} circuit shown in Fig. 3 which is only possible due to the coordinate transformation (7). In particular, the QSP circuit computing the unitaries V_j depends on the block-encoding oracle U_C shown in Fig. 4b encoding the Hermitian C_j , Eq. (13), where C_j is normalized as

$$C_j \rightarrow C_j/\|C_{\max}\|, \quad (17a)$$

$$\|C_{\max}\| = \|A_H + k_{\max}A_L\|. \quad (17b)$$

Each matrix C_j is represented by a sum of two Hermitians,

A_H and B_m , and depends on the sine function $\sin(\theta_j)$. Therefore, the oracle U_C is constructed as an LCU combining two subcircuits, U_{A_H} and U_{B_m} , and an extra subcircuit computing the sine function, Fig. 4c. In particular, the coordinate transformation (7) is necessary to significantly simplify the encoding of the dependence on the Fourier coordinate k by using the subcircuit 4c. The implementation of the block-encoding oracles U_{A_H} and U_{B_m} is problem-specific and depends on the structure of the original non-Hermitian generator A used in Eq. (1).

The oracle U_C is a part of the iterate Q shown in Fig. 4a, which performs qubitization.²¹ The qubitization is used to transform each eigenvalue of the block-encoded matrix C_j within its own Hilbert subspace. Thus, all matrix eigenvalues are transformed in their own disjoint two-dimensional subspaces which allows us to build different powers of the encoded matrix. In this way, we obtain a Grover-like search parallelized over all matrix eigenvalues. More precisely, the qubitization is implemented by using the reflection operator, represented by the last six gates in Fig. 4a. The latter must perform the reflection with respect to any ancillary qubit state orthogonal to the state entangled with the encoded matrices C_j . In our case, each matrix C_j for a particular j is entangled with the state $|j\rangle_{r_k}|0\rangle_{a_{be}}$. Since we want to implement the qubitization for the matrices C_j with all $j = 0, 1, \dots, N_k - 1$ in parallel, we perform the reflection only with respect to $|0\rangle_{a_{be}}$ independently of the state of the register r_k . This ensures that the QSP circuit computes the unitaries V_j for all j at once. Finally, it is worth emphasizing that the QSP in the formulation described in Refs. 21, which is used in this paper, is full-coherent and, thus, does not require AA.

C. LCHS scaling

The selector S makes the main contribution to the cost of the LCHS algorithm, because S scales with time. In particular, since S is implemented by using a QSP circuit, its query complexity in terms of the number of calls to the block-encoding oracle U_C is

$$\mathcal{O}(\|C_{\max}\|t + \log_2 \epsilon_{\text{QSP}}^{-1}), \quad (18)$$

where the simulated time t is multiplied by the spectral norm $\|C_{\max}\|$ because the encoded matrices C_j are normalized according to Eq. (17). An important remark here is that $\|C_{\max}\|$ can grow linearly with k_{\max} . To keep this dependence explicitly, we rewrite Eq. (18) as

$$\mathcal{O}(k_{\max}\|\bar{C}_{\max}\|t + \log_2 \epsilon_{\text{QSP}}^{-1}), \quad (19a)$$

$$\|\bar{C}_{\max}\| = k_{\max}^{-1}\|C_{\max}\|. \quad (19b)$$

Here, according to Eq. (16), the maximum value of the Fourier coordinate, k_{\max} , scales as

$$k_{\max} = \mathcal{O}(\epsilon_{\text{LCHS}}^{-1}) \quad (20)$$

if one uses the special kernel (6). On the other hand, according to Eq. (15), this scaling is improved exponentially,

$$k_{\max} = \mathcal{O}\left(\left(\log_2[\epsilon_{\text{LCHS}}^{-1}]\right)^{1/\beta}\right), \quad (21)$$

if one applies the kernel (5).

Ideally, the selector is constructed as a single QSP circuit where the QSP angles are computed for the normalized time interval $t_{\text{qsp}} = \|\bar{C}_{\text{max}}\|t$, which can be quite large because of the dependence on the matrix spectral norm. Since the computation of the QSP angles for large t_{qsp} is numerically problematic,^{24,25} it may be necessary to split t_{qsp} on N_{int} equal intervals. Then, the QSP angles are computed for a shorter time interval $t_{\text{qsp}}/N_{\text{int}}$. The QSP error is accumulated with N_k and N_{int} . To have the total QSP error be close to the truncation error ϵ_{LCHS} , the local error ϵ_{QSP} for a single time interval $t_{\text{qsp}}/N_{\text{int}}$ should scale at least as

$$\epsilon_{\text{QSP}} = \mathcal{O}(\epsilon_{\text{LCHS}}/(N_k N_{\text{int}})). \quad (22)$$

This results in the following complexity of the LCHS selector

$$\mathcal{O}(k_{\text{max}} \|\bar{C}_{\text{max}}\|t + N_{\text{int}} \log_2 [N_k N_{\text{int}} \epsilon_{\text{LCHS}}^{-1}]). \quad (23)$$

Since the trapezoidal rule was used for the discretization of the LCHS integral (3), the discretized step in the Fourier space should be small enough to make the discretization error close to the truncation error ϵ_{LCHS} . This imposes the following condition on N_k (see Sec. II in Supplemental Material in Ref. 16):

$$N_k = \mathcal{O}\left(\epsilon_{\text{LCHS}}^{-1/2} k_{\text{max}}^{3/2} \|A_L\|t\right). \quad (24)$$

If an efficient block-encoding of the matrices A_L and A_H is provided, then each call to the oracle U_C requires

$$Q_{\text{BE}} = \mathcal{O}(n_k + \text{polylog}(N_x, \zeta)) \quad (25)$$

gates where ζ is the maximum number of nonzero elements in any row or column of the matrices A_L and A_H , and the additive term n_k appears due to the subcircuit 4c computing the sine function. The scaling of the selector S becomes

$$Q_{\text{sel}} = \mathcal{O}(Q_{\text{BE}} [k_{\text{max}} \|\bar{C}_{\text{max}}\|t + Q_{\epsilon}]), \quad (26a)$$

$$Q_{\epsilon} = N_{\text{int}} \log_2 \left(\epsilon_{\text{LCHS}}^{-3/2} k_{\text{max}}^{3/2} \|A_L\|t N_{\text{int}} \right), \quad (26b)$$

where the dependence of k_{max} on ϵ_{LCHS} is described either by Eq. (20), or Eq. (21) depending on the chosen LCHS kernel.

As shown in Ref. 17, if the oracle $U_{\sqrt{w}}$ computing the LCHS weights is implemented using QSVT circuits, then the scaling of the weight computation including AA is

$$Q_w = \mathcal{O}\left(n_k \left[k_{\text{max}}^{3/2} \epsilon_{\text{LCHS}}^{-1} \right]\right), \quad (27)$$

assuming that the error of the weight computation is of the order of ϵ_{LCHS} .

Finally, the scaling of the entire LCHS algorithm is

$$Q_{\text{LCHS}} = \mathcal{O}\left(\frac{\|\psi(0)\|}{\|\psi(t)\|} (Q_{\text{sel}} + Q_w)\right), \quad (28)$$

where the term Q_{sel} , Eq. (26), is the dominant one because of its dependence on the simulated time t . Here, the multiplicative factor $\|\psi(0)\|/\|\psi(t)\|$ takes into account the decrease of the LCHS success probability due to the decay of the simulated signal ψ in time. This happens because of the dissipation in the considered nonunitary problem (1).

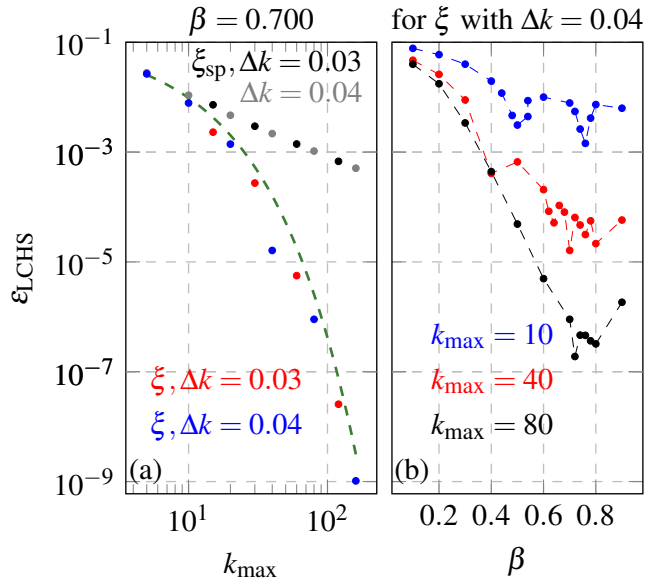


FIG. 5: Plots showing results from LCHS simulations of the ADE for $t = 0.8$ without invoking the LCHS circuit, i.e. classical simulations of the LCHS equation (10). (a): Plot showing the dependence of ϵ_{LCHS} on k_{max} in the LCHS simulations using the special kernel (6) (black and gray markers) and the improved kernel (5) with various Δk and with $\beta = 0.7$ (colored markers). The green dashed line approximates the error with the fitting function (32). (b): Plot showing the dependence of ϵ_{LCHS} on β in the LCHS simulations with the improved kernel (5) for various k_{max} and for $\Delta k = 0.04$.

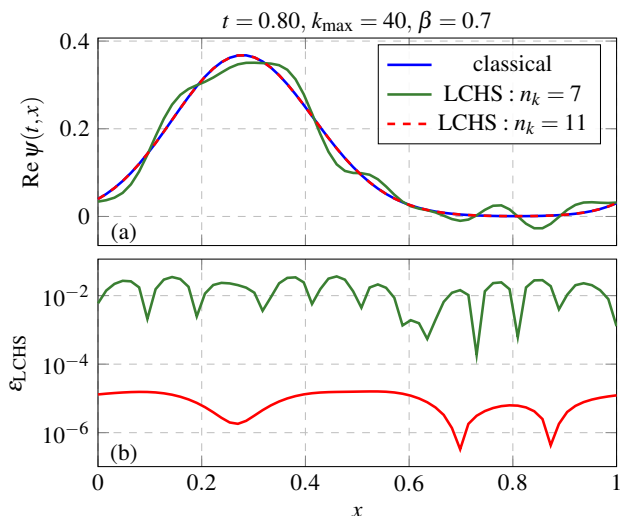


FIG. 6: (a): Plot showing the comparison between classical simulations (blue line) and LCHS simulations using the LCHS circuit 2 for various n_k (green and red lines). (b): Plot showing the error in the LCHS simulations.

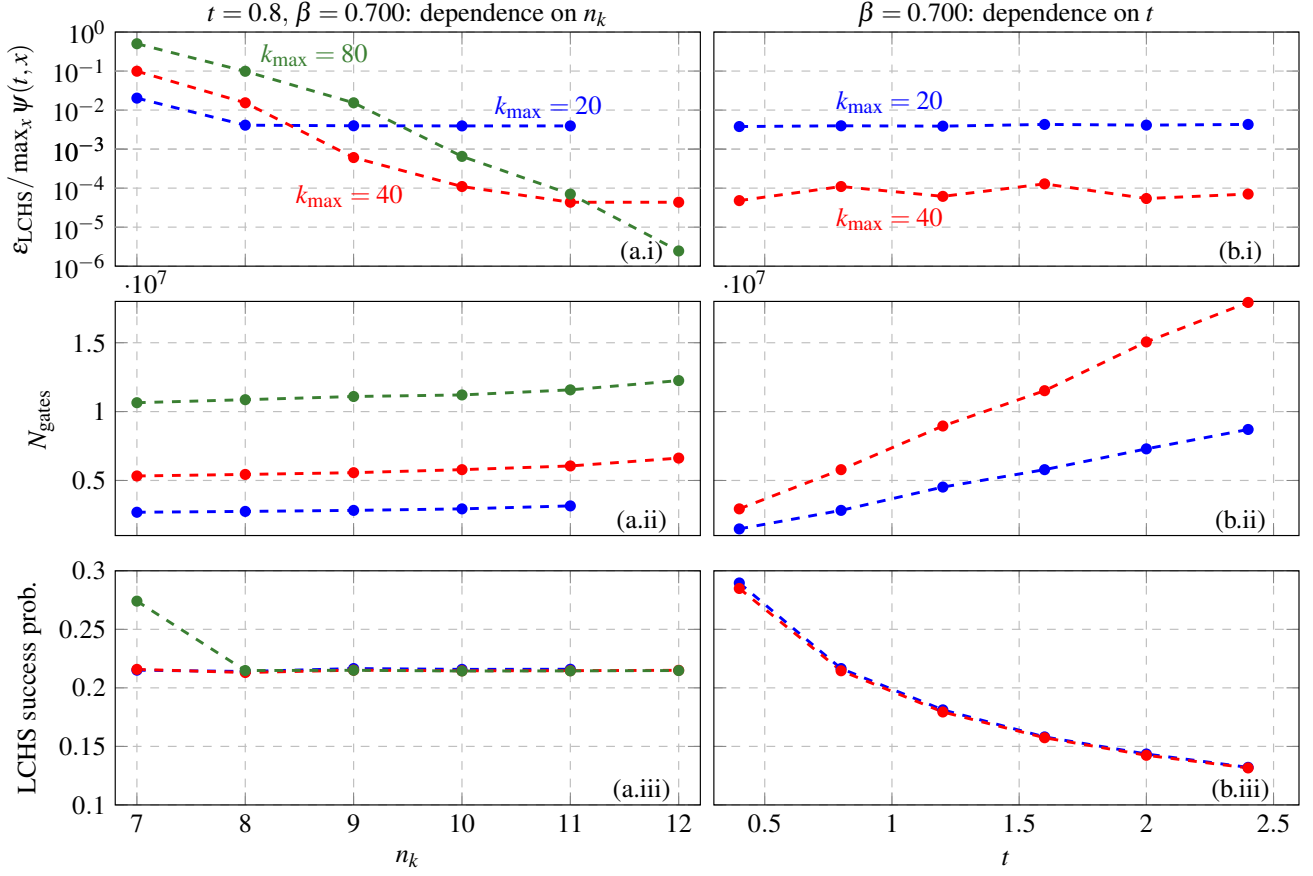


FIG. 7: Plots showing the dependence of the normalized LCHS error (a.i), the number of STMC gates (a.ii), and the success probability of the LCHS circuit (a.iii) on n_k in the LCHS simulations using the circuit 2 for various k_{\max} . Plots showing the dependence of the error (b.i), N_{gates} (b.ii), and the success probability (b.iii) on t for various k_{\max} . For $k_{\max} = 20$, the cases with $t = 0.4$ and $t = 0.8$ have $n_k = 9$, the cases with $t = 1.2$ and $t = 1.6$ have $n_k = 10$, and so on. The corresponding values of n_k are increased by one for $k_{\max} = 40$.

III. NUMERICAL SIMULATIONS

To investigate the scaling and the success probability of the described LCHS circuit, we simulate the advection-diffusion equation (ADE) with a uniform velocity $v = 1.0$ and diffusivity $D = 0.01$:

$$\partial_t \psi = -v \partial_x \psi + D \partial_x^2 \psi. \quad (29)$$

The detailed quantum circuit for modeling this equation is given in Ref. 26. The initial condition $\psi(0, x)$ is a Gaussian centered at $x = 0.5$ with the width 0.05. The simulated domain, $x = [0, 1]$, with periodic boundary conditions is discretized with N_x spatial points. After the discretization, Eq. (29) is recast as Eq. (1) with the following matrix:

$$A_{i_r i_c} = - \begin{cases} c_{-1}, & i_c = i_r - 1, \\ c_0, & i_c = i_r, \\ c_{+1}, & i_c = i_r + 1, \end{cases} \quad (30)$$

where $i_r, i_c = 0, 1, \dots, (N_x - 1)$, $A_{(N_x-1), N_x} \equiv A_{(N_x-1), 0}$, $A_{0, -1} \equiv A_{0, (N_x-1)}$, and the constant scalars are

$$c_0 = -\frac{2D}{\Delta x^2}, \quad c_{\pm 1} = \left(\frac{D}{\Delta x^2} \mp \frac{v}{2\Delta x} \right), \quad \Delta x = (N_x - 1)^{-1}. \quad (31)$$

For the LCHS simulations, the matrix A is decomposed into Hermitian components A_L and A_H according to Eq. (4), and then one solves Eq. (10) where the LCHS operator U_{LCHS} is represented by the weighted sum (11).

First of all, we solve Eq. (10) directly without invoking the LCHS circuit 2. The results of these simulations for various LCHS kernels and various values of the scalar β are shown in Fig. 5. In particular, one can see there that the scaling of the truncation error ϵ_{LCHS} with k_{\max} can be exponentially improved by using the kernel (5). In this case, the scaling can be approximated by the function

$$\epsilon_{\text{LCHS}} = 0.119 \exp(-0.5 k_{\max}^\beta), \quad (32)$$

which numerically confirms the theoretical scaling (15). Moreover, we have some flexibility in the choice of the scalar parameter β in the kernel ξ . According to Fig. 5b, its value

should be taken in the interval between 0.7 and 0.8, which is consistent with Ref. 18.

Now, to test the LCHS method mapped on the LCU circuit 2 using the coordinate transformation (7) and the kernel (5), we simulate this circuit with different k_{\max} and n_k . The circuit is constructed using single-target multicontrolled (STMC) gates such as X , H , R_y , and R_z gates controlled by multiple qubits. According to Refs. 27 and 28, an STMC gate controlled by n_c qubits can be represented by a circuit with $\mathcal{O}(n_c)$ elementary gates without using ancillae.

The signal $\psi(t, x)$ at $t = 0.8$ and the corresponding error in the LCHS simulation with the circuit 2 are shown in Fig. 6. In particular, one can see that it is possible to decrease the error up to around 10^{-5} using $k_{\max} = 40$ with $n_k = 11$. The scaling of the LCHS error, the number of STMC gates in the circuit, and the circuit success probability are shown in Fig. 7 as functions of k_{\max} , n_k , and the simulated time interval t . Clearly, by increasing k_{\max} and n_k for a given time instant t , one can exponentially increase the LCHS precision. At the same time, the number of gates in the LCHS circuit increases linearly with k_{\max} and only logarithmically with N_k , while the success probability of the circuit stays near the same level. This is consistent with Eqs. (25) and (26). On the other hand, the circuit success probability decreases with time because the simulated signal $\psi(t, x)$ decays in time due to the imposed diffusivity D . Finally, the number of gates in the circuit grows linearly with time while the LCHS precision stays at nearly the same level. Hence, we have a near-optimal quantum algorithm for modeling the advection-diffusion equation, which scales linearly with time and whose error decreases exponentially with k_{\max} .

IV. CONCLUSIONS

In this work, an efficient quantum algorithm based on the Linear Combination of Hamiltonian Simulations (LCHS) has been proposed for simulating dissipative initial-value problems. In this method, a nonunitary operator represented by an exponential function of a non-Hermitian generator is approximated by a weighted sum of Hamiltonian evolutions that depend on the Hermitian components of the generator and on an additional Fourier coordinate. By recasting the Fourier coordinate as a trigonometric function, we derived an efficient encoding of the LCHS sum into a quantum circuit. Due to this, the circuit scales linearly with the simulated time and logarithmically with the number of terms in the sum. The quantum circuit was tested by modeling the advection-diffusion equation with a uniform velocity and diffusivity, and the numerical simulations confirmed the scaling of the proposed circuit. The proposed encoding of dissipative problems can be used for solving a wide class of nonunitary differential equations including the Liouville equation and various linear embedding techniques of nonlinear problems.

ACKNOWLEDGMENTS

This work, LLNL-JRNL-2001345, was supported by the U.S. Department of Energy (DOE) Office of Fusion Energy Sciences “Quantum Leap for Fusion Energy Sciences” Project No. FWP-SCW1680 at Lawrence Livermore National Laboratory (LLNL). Work was performed under the auspices of the U.S. DOE under LLNL Contract DE-AC52-07NA27344. This research used resources of the National Energy Research Scientific Computing Center, a DOE Office of Science User Facility supported by the Office of Science of the U.S. Department of Energy under Contract No. DE-AC02-05CH11231 using NERSC award FES-ERCAP0028618.

- ¹H. Krovi, Improved quantum algorithms for linear and nonlinear differential equations, *Quantum* 7 (2023) 913. doi:10.22331/q-2023-02-02-913.
URL <http://dx.doi.org/10.22331/q-2023-02-02-913>
- ²N. Linden, A. Montanaro, C. Shao, Quantum vs. classical algorithms for solving the heat equation, *Communications in Mathematical Physics* 395 (2) (2022) 601–641.
- ³A. Ambainis, Variable time amplitude amplification and quantum algorithms for linear algebra problems, in: C. Dürr, T. Wilke (Eds.), 29th International Symposium on Theoretical Aspects of Computer Science (STACS 2012), Vol. 14 of Leibniz International Proceedings in Informatics (LIPIcs), Schloss Dagstuhl–Leibniz-Zentrum fuer Informatik, Dagstuhl, Germany, 2012, pp. 636–647. doi:10.4230/LIPIcs.STACS.2012.636.
URL <http://drops.dagstuhl.de/opus/volltexte/2012/3426>
- ⁴A. M. Childs, R. Kothari, R. D. Somma, Quantum algorithm for systems of linear equations with exponentially improved dependence on precision, *SIAM Journal on Computing* 46 (6) (2017) 1920–1950. arXiv:<https://doi.org/10.1137/16M1087072>, doi:10.1137/16M1087072.
URL <https://doi.org/10.1137/16M1087072>
- ⁵S. Chakraborty, A. Gilyén, S. Jeffery, The power of block-encoded matrix powers: Improved regression techniques via faster hamiltonian simulation, *Schloss Dagstuhl – Leibniz-Zentrum für Informatik*, 2019. doi:10.4230/LIPIcs.ICALP.2019.33.
URL <https://drops.dagstuhl.de/entities/document/10.4230/LIPIcs.ICALP.2019.33>
- ⁶D. An, L. Lin, Quantum linear system solver based on time-optimal adiabatic quantum computing and quantum approximate optimization algorithm, *ACM Transactions on Quantum Computing* 3 (2) (Mar. 2022). doi:10.1145/3498331.
URL <https://doi.org/10.1145/3498331>
- ⁷P. C. Costa, D. An, Y. R. Sanders, Y. Su, R. Babbush, D. W. Berry, Optimal scaling quantum linear-systems solver via discrete adiabatic theorem, *PRX Quantum* 3 (2022) 040303. doi:10.1103/PRXQuantum.3.040303.
URL <https://link.aps.org/doi/10.1103/PRXQuantum.3.040303>
- ⁸D. Fang, L. Lin, Y. Tong, Time-marching based quantum solvers for time-dependent linear differential equations, *Quantum* 7 (2023) 955. doi:10.22331/q-2023-03-20-955.
URL <https://doi.org/10.22331/q-2023-03-20-955>
- ⁹P. Over, S. Bengoechea, P. Brearley, S. Laizet, T. Rung, Quantum algorithm for the advection-diffusion equation with optimal success probability (2024). arXiv:2410.07909.
URL <https://arxiv.org/abs/2410.07909>
- ¹⁰R. Demirdjian, D. Gunlycke, C. A. Reynolds, J. D. Doyle, S. Tafur, Variational quantum solutions to the advection–diffusion equation for applications in fluid dynamics, *Quantum Information Processing* 21 (9) (2022) 322. doi:10.1007/s11128-022-03667-7.
URL <https://doi.org/10.1007/s11128-022-03667-7>
- ¹¹J. Ingelmann, S. S. Bharadwaj, P. Pfeiffer, K. R. Sreenivasan, J. Schumacher, Two quantum algorithms for solving the one-dimensional advection–diffusion equation, *Computers & Fluids* 281 (2024) 106369.

- doi:10.1016/j.compfluid.2024.106369.
URL <http://dx.doi.org/10.1016/j.compfluid.2024.106369>
- ¹²S. Jin, N. Liu, Y. Yu, Quantum simulation of partial differential equations via Schrödingerisation (2022). arXiv:2212.13969.
URL <https://arxiv.org/abs/2212.13969>
- ¹³S. Jin, N. Liu, Y. Yu, Quantum simulation of partial differential equations: Applications and detailed analysis, *Phys. Rev. A* 108 (2023) 032603. doi:10.1103/PhysRevA.108.032603.
URL <https://link.aps.org/doi/10.1103/PhysRevA.108.032603>
- ¹⁴J. Hu, S. Jin, N. Liu, L. Zhang, Quantum circuits for partial differential equations via Schrödingerisation (2024). arXiv:2403.10032.
URL <https://arxiv.org/abs/2403.10032>
- ¹⁵Z. Lu, Y. Yang, Quantum computing of reacting flows via Hamiltonian simulation, *Proceedings of the Combustion Institute* 40 (1) (2024) 105440. doi:<https://doi.org/10.1016/j.proci.2024.105440>.
URL <https://www.sciencedirect.com/science/article/pii/S1540748924002487>
- ¹⁶D. An, J.-P. Liu, L. Lin, Linear combination of hamiltonian simulation for nonunitary dynamics with optimal state preparation cost, *Phys. Rev. Lett.* 131 (2023) 150603. doi:10.1103/PhysRevLett.131.150603.
URL <https://link.aps.org/doi/10.1103/PhysRevLett.131.150603>
- ¹⁷I. Novikau, I. Joseph, Quantum algorithm for the advection-diffusion equation and the Koopman-von Neumann approach to nonlinear dynamical systems, *Computer Physics Communications* 309 (2025) 109498. doi:<https://doi.org/10.1016/j.cpc.2025.109498>.
URL <https://www.sciencedirect.com/science/article/pii/S0010465525000013>
- ¹⁸D. An, A. M. Childs, L. Lin, Quantum algorithm for linear non-unitary dynamics with near-optimal dependence on all parameters (2023). arXiv:2312.03916.
- ¹⁹S. Jin, N. Liu, C. Ma, On schrödingerization based quantum algorithms for linear dynamical systems with inhomogeneous terms (2024). arXiv:2402.14696.
URL <https://arxiv.org/abs/2402.14696>
- ²⁰G. H. Low, I. L. Chuang, Optimal Hamiltonian simulation by quantum signal processing, *Physical Review Letters* 118 (2017) 010501. doi:10.1103/PhysRevLett.118.010501.
URL <https://link.aps.org/doi/10.1103/PhysRevLett.118.010501>
- ²¹G. H. Low, I. L. Chuang, Hamiltonian simulation by qubitization, *Quantum* 3 (2019) 163. doi:10.22331/q-2019-07-12-163.
URL <https://doi.org/10.22331/q-2019-07-12-163>
- ²²Y. Sato, H. Tezuka, R. Kondo, N. Yamamoto, Quantum algorithm for partial differential equations of non-conservative systems with spatially varying parameters (2024). arXiv:2407.05019.
URL <https://arxiv.org/abs/2407.05019>
- ²³G. Brassard, P. Høyer, M. Mosca, A. Tapp, Quantum amplitude amplification and estimation, *Quantum Computation and Information* 305 (2002) 53–74. doi:10.1090/conm/305/05215.
URL <http://dx.doi.org/10.1090/conm/305/05215>
- ²⁴J. Haah, Product decomposition of periodic functions in quantum signal processing, *Quantum* 3 (2019) 190. doi:10.22331/q-2019-10-07-190.
URL <http://dx.doi.org/10.22331/q-2019-10-07-190>
- ²⁵S. E. Skelton, Mostly harmless methods for qsp-processing with laurent polynomials (2024). arXiv:2408.04321.
URL <https://arxiv.org/abs/2408.04321>
- ²⁶Near-optimal LCHS quantum circuits, <https://github.com/QuCF/QuCF/wiki/OPT%E2%80%9090LCHS> (2024).
- ²⁷A. Barenco, C. H. Bennett, R. Cleve, D. P. DiVincenzo, N. Margolus, P. Shor, T. Sleator, J. A. Smolin, H. Weinfurter, Elementary gates for quantum computation, *Phys. Rev. A* 52 (1995) 3457–3467. doi:10.1103/PhysRevA.52.3457.
URL <https://link.aps.org/doi/10.1103/PhysRevA.52.3457>
- ²⁸B. Claudon, J. Zylberman, C. Feniou, F. Debbasch, A. Peruzzo, J.-P. Piquemal, Polylogarithmic-depth controlled-not gates without ancilla qubits, *Nature Communications* 15 (1) (2024) 5886. doi:10.1038/s41467-024-50065-x.
URL <https://doi.org/10.1038/s41467-024-50065-x>